
ScatterSample: Diversified Label Sampling for Data Efficient Graph Neural Network Learning

Anonymous Author(s)

Anonymous Affiliation

Anonymous Email

Abstract

1
2 What target labels are most effective for graph neural network (GNN) training? In
3 some applications where GNNs excel-like drug design or fraud detection, labeling
4 new instances is expensive. We develop a data-efficient active sampling framework,
5 ScatterSample, to train GNNs under an active learning setting. ScatterSample
6 employs a sampling module termed DiverseUncertainty to collect instances with
7 large uncertainty from different regions of the sample space for labeling. To
8 ensure diversification of the selected nodes, DiverseUncertainty clusters the high
9 uncertainty nodes and selects the representative nodes from each cluster. Our
10 ScatterSample algorithm is further supported by rigorous theoretical analysis
11 demonstrating its advantage compared to standard active sampling methods that
12 aim to simply maximize the uncertainty and not diversify the samples. In particular,
13 we show that ScatterSample is able to efficiently reduce the model uncertainty over
14 the whole sample space. Our experiments on five datasets show that ScatterSample
15 significantly outperforms the other GNN active learning baselines, specifically it
16 reduces the sampling cost by up to 50% while achieving the same test accuracy.

17 1 Introduction

18 How to spot the most effective labeled nodes for GNN training? Graph neural networks (GNN)
19 [KW16; Vel+17; Wu+19a] which employ non-linear and parameterized feature propagation [ZG02]
20 to compute graph representations, have been widely employed in a broad range of learning tasks
21 and achieved state-of-art-performance in node classification, link prediction and graph classification.
22 Training GNNs for node classification in the supervised learning setup typically requires a large
23 number of labeled examples such that the GNN can learn from diverse node features and node
24 connectivity patterns. However, labeling costs can be expensive which inhibits the possibility of
25 acquiring a large number of node labels. For example, the GNNs can be used to assist the drug
26 design. However, evaluating the properties of a molecule is time consuming. It usually takes one
27 to two weeks for evaluation using the current simulation tools, not to mention the cost spent on the
28 laboratory experiments.

29 Active learning (AL) aims at maximizing the generalization performance under a constrained labeling
30 budget [Set09]. AL algorithms choose which training instances to use as labeled targets to maximize
31 the performance of the learned model. Previous research in AL algorithms for GNN training can be
32 categorized with respect to whether the AL methods take into account the model weights (model
33 aware) or can be applied to any model (model agnostic). Model agnostic algorithms label a represen-
34 tative subset of the nodes such that the labeled nodes can cover the whole sample space [Wu+19b;
35 Zha+21]. Model aware AL algorithms leverage the GNN model to compute the node uncertainty,
36 which combines both the input features and graph structure [CZC17; Gao+18]. AL then picks the
37 nodes with the highest uncertainty.

38 However, maximizing the uncertainty of the labeled nodes may not balance the exploration and
39 exploitation of the classification boundary [KVAG19]. For example, if there exist a group of nodes
40 close to the classification boundary but are clustered in a small region of the graph, just labeling
41 the most uncertain nodes could only explore that specific region of the classification boundary,

42 while others are ignored, and the classification boundary is not well explored. Thus, our first main
 43 contribution is to simultaneously consider the node uncertainty and the diversification of the uncertain
 44 nodes over the sample space.

45 **Challenges of diversifying uncertain nodes.** Graph data present additional challenges to diversify
 46 the uncertain nodes. Diversification requires modeling the sample space using carefully selected
 47 representations for the nodes. However, there are two challenges of a suitable node representations.

48 Challenge 1: Sample space for graph data requires a representation which takes both the graph
 49 structure and node features into account (see section sec 4.2).

50 Challenge 2: The representation should be robust to the model trained so far, and not be biased by
 51 the limited amount of available labels.

52 **Our approach.** We develop *ScatterSample* for data-efficient GNN learning. *ScatterSample* allows
 53 us to explore the classification boundary while exploiting the nodes with the highest uncertainty. To
 54 diversify the uncertain samples on graph-structured data, *ScatterSample* includes a *DiverseUncer-*
 55 *tainty* module to address the two challenges above, which clusters the uncertain nodes representations
 56 over the whole sample space.

57 **Our Contributions.** The contributions of our work are
 58 the following.

- 59 • **Insight:** *ScatterSample* is the first method that pro-
 60 poses and implements diversification of the uncertain
 61 samples for data efficient GNN learning.
- 62 • **Effectiveness:** We evaluate *ScatterSample* on five
 63 different graph datasets, where *ScatterSample* saves
 64 up to **50%** labeling cost, while still achieving the
 65 same test accuracy with state-of-the-art baselines.
- 66 • **Theoretical Guarantees:** Our theoretical analysis
 67 proves the superiority of *ScatterSample* over the
 68 standard, uncertainty-sampling method (see Theo-
 69 rem 5.1). Simulation results further confirm our the-
 70 ory.

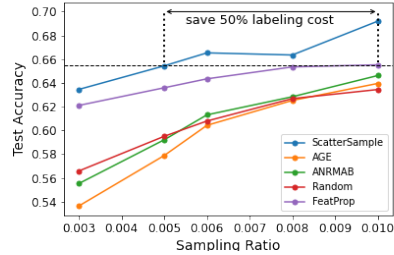


Figure 1: *ScatterSample* wins: test accuracy vs. sampling ratio on the ogbn-products dataset (62M edges).

71 2 Related Work

72 This section will review the uncertainty based active learn-
 73 ing research and implementation of active learning in GNNs.

74 **Active Learning (AL):.** Active learning aims at selecting a subset of training data as labeling
 75 targets such that the model performance is optimized [Set09; Han+14]. Uncertainty sampling is
 76 one major approach of active learning, which labels a group of samples to maximally reduce the
 77 model uncertainty. To achieve this goal, uncertainty sampling selects samples around the decision
 78 boundary [THTS05]. Uncertainty sampling has also been applied to the deep learning field, and
 79 researchers have proposed different methods to measure the uncertainty of samples. For example,
 80 Ducoffe and Precioso [DP18] developed a margin based method which uses the distance from a
 81 sample to its smallest adversarial sample to approximate the distance to the decision boundary.

82 **AL and GNNs:** AL with GNNs requires to consider the graph structure information into the node
 83 selection. Wu et al. [Wu+19b] uses the propagated features followed by K-Medoids clustering of
 84 nodes to select a group of representative instances. Zhang et al. [Zha+21] measures importance of
 85 nodes through combining the diversity and influence scores. However the above approaches do not
 86 account for the learned GNN model, which may limit the generalization performance. Uncertainty
 87 sampling has also been implemented to select nodes. Cai et al. [CZC17] propose to use a weighted
 88 average of the node uncertainty, graph centrality and information density scores. Gao et al. [Gao+18]
 89 further propose a different approach to combine the three features with multi-armed bandit techniques.
 90 Although useful, these approaches aim choose nodes with the highest uncertainty and may be
 91 challenged if the selected nodes are clustered in a small region of the graph, which will not provide
 92 good graph coverage. Our work addresses this limitation by diversifying the selected nodes based on
 93 the graph structure.

3 Preliminaries

Problem Statement . Given a graph $\mathcal{G} = (\mathcal{V}, \mathcal{E})$, where \mathcal{V} is the set of nodes with $N = |\mathcal{V}|$ nodes and \mathcal{E} is the set of edges. The set of nodes is divided into the training set \mathcal{V}_{train} , validation set \mathcal{V}_{valid} and testing set \mathcal{V}_{test} . Each node $v_n \in \mathcal{V}$ is associated with a feature vector $\mathbf{x}_n \in \mathbb{R}^d$ and a label $y_n \in \{1, 2, \dots, C\}$. Let $\mathbf{X} \in \mathbb{R}^{N \times d}$ be the feature matrix of all the nodes in the graph, where the i -th row of \mathbf{X} corresponds to v_n , $\mathbf{y} = (y_1, y_2, \dots, y_n) \in \mathbb{R}^n$ is the vector containing all the labels. To learn the labels of the nodes, we train a GNN model M which maps the graph \mathcal{G} and \mathbf{X} to the prediction of labels $\hat{\mathbf{y}}$.

Active Learning: Active learning picks a subset of nodes $S \subset \mathcal{V}_{train}$ from the training set and query their labels \mathbf{y}_S . A GNN model M_S is trained with respect to the feature matrix \mathbf{X} and \mathbf{y}_S . Given the sampling budget B , the goal of active learning is to find a set S ($|S| \leq B$) such that the generalization loss is minimized, i.e.

$$\arg \min_{S: |S| \leq b} \mathbb{E}_{v_n \in \mathcal{V}_{test}} (\ell(y_n, f(\mathbf{x}_n | \mathcal{G}, M_S))) .$$

3.1 Graph neural networks and message passing

In this section we present the basic operation of the GNN at layer l . With the message passing paradigm, the GNN layer updates for most GNN models can be interpreted as message vectors that are exchanged among neighbors over the edges and nodes in the graph.

For the following let $\mathbf{h}_v^{(l)} \in \mathbb{R}^{d_1}$ be the hidden representation for node v and layer l . Consider ϕ that is a message function combining the hidden representations for nodes v, u . Next, using the message vectors for neighboring edges the node representations are updated as follows

$$\mathbf{h}_v^{(l+1)} = \psi \left(\mathbf{h}_v^{(l)}, \rho(\{\phi(\mathbf{h}_v^{(l)}, \mathbf{h}_u^{(l)}) : (u, v) \in \mathcal{E}\}) \right) \quad (1)$$

where ρ is a reduce function used to aggregate the messages coming from the neighbors of v and ψ is an update function defined on each node to update the hidden node representation for layer $l + 1$. By defining ϕ, ρ, ψ different GNN models can be instantiated [KW16; DBV16; Bro+17; IMG20]. These functions are also parameterized by learnable matrices that are updated during training.

4 Proposed method: ScatterSample

We propose the *ScatterSample* algorithm, which dynamically samples a set of diverse nodes with large uncertainties in order to more efficiently explore the classification boundary during GNN training. At each round, our method calculates the uncertainty for all nodes with the GNN model trained so far. Then, *ScatterSample* clusters the top uncertain nodes and selecting nodes from each cluster to obtain diverse samples. The labels of the selected nodes are queried and used as supervision to continue training the GNN model for the next round. This section explains our method in detail.

4.1 Selecting the uncertain nodes

The uncertainty of a node is measured by the information entropy. Given a trained GNN model at the t -th sampling round, *ScatterSample* first computes the information entropy $\phi_{entropy}(v_n)$ of nodes in \mathcal{V}_{train} based on the current GNN model, i.e.

$$\phi_{entropy}(v_n) = - \sum_{j=1}^C \log(\text{P}[Y_n = j | \mathcal{G}, \mathbf{X}, M]) \text{P}[Y_n = j | \mathcal{G}, \mathbf{X}, M] \quad (2)$$

where $\text{P}[Y_n = j | \mathcal{G}, \mathbf{X}, M]$ is probability that node v_n belongs to class j given the GNN model M . Then, *ScatterSample* ranks all the nodes in order of decreasing uncertainty, and picks the ones with the largest information entropy into a candidate set $\mathcal{C}_t \subset \mathcal{V}_{train}$. Different than traditional AL techniques that select training targets solely based on uncertainty, we then move on to pick a diverse subset of the uncertain nodes over the sampling space.

4.2 Diversifying uncertain nodes

Our goal is to ensure the diversity of selected nodes for labeling, by exploring the node distribution over the sample space. At this point naturally, the question arises *How to model the sample space?* We need a representation for nodes to define the space, based on which we could measure the samples' distances. A straightforward approach is to use the GNN embedding space since the classification

139 boundary is directly depicted there. However, GNN embeddings fail to address the two challenges in
 140 the introduction section.

141 First, with active learning, a limited number of labeled nodes are available in the initial stages.
 142 Hence, only the already labeled nodes may have reliable GNN embeddings and biased subsequent
 143 samples. Second, GNN embeddings for node classification may not carry enough information for
 144 diversification. GNNs usually do not have an MLP layer connecting to the output. The final GNN
 145 outputs of uncertain nodes are not diverse enough since the high uncertain nodes may have similar
 146 class probabilities (class probabilities close to uniform). Conversely, embeddings of intermediate
 147 GNN layers may have an appropriate dimension but lack information of the expanded ego-network.

148 These drawbacks are confirmed in Sec. 6.2, where we show that using GNN embeddings as proxy
 149 representations leads to a performance drop. Moreover, different from other machine learning
 150 problems, the nodes are correlated with each other, and we also need to take the graph structure into
 151 account when diversifying the samples. Hence, to address all these considerations we will employ a
 152 k -step propagation of the original node features based on the graph structure as a proxy representation
 153 for the nodes. The k -step propagation of nodes $\mathbf{X}^{(k)} = (\mathbf{x}_1^{(k)}, \mathbf{x}_2^{(k)}, \dots, \mathbf{x}_N^{(k)})$ is defined as follows

$$\mathbf{X}^{(k)} := \mathbf{S}\mathbf{X}^{(k-1)} \quad (3)$$

154 where \mathbf{S} is the normalized adjacency matrix, and $\mathbf{X}^{(0)}$ are the initial node features. The operation
 155 in (3) is efficient and amenable to a mini-batch implementation. Such representations are well-known
 156 to succinctly encode the node feature distribution and graph structure. Next, we calculate the proxy
 157 representations for the candidate high uncertainty nodes in the set \mathcal{C}_t . To maximize the diversity of
 158 the samples, we cluster the proxy representations in \mathcal{C}_t using k -means++ into B_t clusters [AV06],
 159 and select the nodes closest to the cluster centers for labeling, by using the L_2 distance metric. One
 160 node from each cluster is selected that amounts to B_t samples.

Algorithm 1 ScatterSample Algorithm

1: **Input:** \mathcal{V}_{train} , GNN model M , number of propagation layers k , number of sampling round T ,
 sampling redundancy r , initial sampling budget B_0 and total sampling budget B .

2: Initialize $S = \emptyset$

3: Compute $\mathbf{x}_n^{(k)} \forall n \in \mathcal{V}_{train}$ as in (3).

4: **Initial Sampling:**

5: Use k -means++ to cluster $\{\mathbf{x}_n^{(k)}\}$ into B_0 clusters.

6: Add a node closest to the cluster center per cluster to S .

7: Query the labels of nodes $v_n \in S$, denoted by \mathbf{y}_S .

8: Train model M using $(\mathbf{y}_S, \mathbf{X}, \mathcal{G})$.

9: **Dynamic Sampling:**

10: Initialize sampling round $t = 1$

11: **while** $t < T$ **do**

12: Let $B_t = \min(B - |S|, (B - B_0)/T)$

13: Use the **DiverseUncertainty** algorithm to select S_t

14: Query the labels of S_t , and update $S = S \cup S_t$.

15: Train model M over $(\mathbf{y}_S, \mathbf{X}, \mathcal{G})$. Update $t = t + 1$.

16: **end while**

161 Clearly, the size of the candidate set $|\mathcal{C}_t| \geq B_t$, however deciding how many candidate nodes to
 162 choose from is important. We parameterize the size as a multiple of the selected nodes namely
 163 $|\mathcal{C}_t| = rB_t$, where $r > 1$ is the sampling redundancy. If r is too small, the selected nodes are closer
 164 to the classification boundary (have larger information entropy) but the nodes selected may not be
 165 diverse enough. On the other hand, if r is too large, the set will be diverse, but the selected nodes may
 166 be far away from the classification boundary. Therefore, it is critical to pick a suitable r to achieve
 167 a sweet point between diversity and uncertainty. We leave the discussion of choosing r to Sec. 6.2.
 168 Besides empirical validation with experiments in five real datasets (see Sec. 6), our diversification
 169 approach is theoretically motivated (see Sec. 5).

170 The pseudo code of ScatterSample is shown in Algorithm 1. ScatterSample is a multiple rounds
 171 sampling scheme, which includes an initial sampling step and dynamic sampling steps. ScatterSample

Algorithm 2 DiverseUncertainty Algorithm

- 1: **Input:** $\mathcal{V}_{train}, \{\mathbf{x}_n^{(k)} \forall n \in \mathcal{C}_t\}, r, B_t$
 - 2: Compute $\phi_{entropy}(v) \forall v \in \mathcal{V}_{train}$; see 2).
 - 3: $\mathcal{C}_t \leftarrow \{r B_t \text{ nodes with largest } \phi_{entropy}(v)\}$.
 - 4: Use k -means++ to cluster the $\mathbf{x}_n^{(k)}$ (for all $n \in \mathcal{C}_t$) into B_t clusters.
 - 5: $S_t \leftarrow \emptyset$
 - 6: **for** $j = 1, 2, \dots, B_t$ **do**
 - 7: Compute the cluster center \mathbf{v}_j of cluster j
 - 8: Pick node $x \leftarrow \arg \min_{n \in \mathcal{C}_t} \|\mathbf{x}_n^{(k)} - \mathbf{v}_j\|$
 - 9: $S_t \leftarrow S_t \cup \{x\}$
 - 10: **end for**
 - 11: **Return** S_t
-

172 first computes the k -step features propagation of all the nodes in the training set using (3), and clusters
 173 them into B_0 clusters, where B_0 is the initial sampling budget. Then, *ScatterSample* picks the nodes
 174 closest to the cluster centers as the initial training samples and queries their labels. The purpose of
 175 clustering k -step feature propagations is to enforce the initial training set to spread out over the whole
 176 sample space. It is also helpful to explore the classification boundary since if the initial sampled
 177 nodes are not diverse enough, we cannot picture the classification boundary of the regions that are far
 178 away from the initial training samples. *ScatterSample* repeats the dynamic sampling described in
 179 Algorithm 2 until the sampling budget B is exhausted. The next section fortifies our diversification
 180 method with theoretical guarantees.

181 **5 Theoretical analysis**

182 In Sec. 6.2, we have shown that DiverseUncertainty is significantly better than Uncertainty algorithm.
 183 In this section, we provide theoretical analysis and simulation results to demonstrate the benefits of
 184 DiverseUncertainty and explains why MaxUncertainty algorithm may fail. The results presented
 185 here give a theoretical basis for the superiority of our method as established in the experiments in
 186 Section 6.

187 **5.1 Analysis setup**

188 For the analysis, we employ the Gaussian Process (GP) model [O’H78]. GP models offer a flexible
 189 approach to model complex functions and are robust to small sample sizes [See04]. Moreover, the
 190 uncertainty of the prediction can be easily computed using a GP model. Neural network models
 191 and GNNs interpolate the observed samples, while GPs provide a robust framework to interpolate
 192 samples, that is amenable to analysis.

193 Assume the label $y_i \in \mathbb{R}$ is dependent on the propagated features $\mathbf{x}_i^{(k)}$ through a GP model. The
 194 label y_i is modeled by a Gaussian Process, where $(\mathbf{y} \mid \mathbf{X}^{(k)}) \sim N(\mathbf{1}\mu, \mathbf{K}(\mathbf{X}^{(k)}))$ and $\mathbf{K}(\mathbf{X}^{(k)})$
 195 is the Gaussian kernel matrix. The kernel is parameterized by $\mathbf{K}_{ij}(\mathbf{X}^{(k)}) = K(\mathbf{x}_i^{(k)}, \mathbf{x}_j^{(k)}) =$
 196 $\exp\left(-\frac{1}{2}(\mathbf{x}_i^{(k)} - \mathbf{x}_j^{(k)})^T \Sigma^{-1}(\mathbf{x}_i^{(k)} - \mathbf{x}_j^{(k)})\right)$, where $\Sigma = \text{diag}(\theta_1, \theta_2, \dots, \theta_d)$. Consider that the
 197 sample space of $\mathbf{x}^{(k)}$ can be clustered into m clusters $\mathcal{S}_1, \mathcal{S}_2, \dots, \mathcal{S}_m$, and denote the cluster centers as
 198 $\mathbf{c}_1, \mathbf{c}_2, \dots, \mathbf{c}_m$. Without loss of generality, denote the radius of the cluster, $d_1 \leq d_2 \leq d_3 \leq \dots < d_m$.
 199 The clusters are well separated and the distance between the cluster centers are larger than δ , i.e.
 200 $\min_{i \neq j} \|\mathbf{c}_i - \mathbf{c}_j\|_2 \geq \delta$ ($\delta > 2d_m$). Moreover, we consider that there does not exist a cluster
 201 dominating the sample space, $d_m^2 \leq \tau \sum_{j=1}^{m-1} d_j^2$ and the samples are uniformly distributed over the
 202 clusters.

203 **5.2 MaxUncertainty vs DiverseUncertainty**

204 Here, we show that DiverseUncertainty could significantly achieves smaller mean squared error
 205 (MSE) compared to MaxUncertainty. Without loss of generality we consider m clusters and the
 206 following definitions.

- 207 • **MaxUncertainty** Select $2m$ most uncertain samples.

208

- **DiverseUncertainty** Select the 2 most uncertain samples from each cluster.

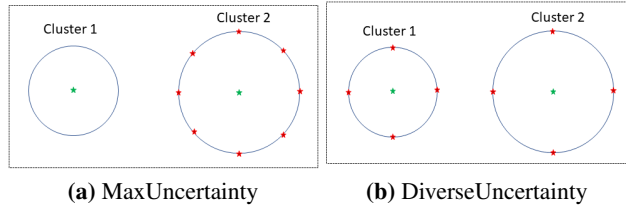


Figure 2: The area enclosed by the blue circles is the sample space of propagated features (2D case). The green stars are sampled nodes during initial sampling (cluster center). The red stars are the sampled nodes during uncertainty sampling. (a) MaxUncertainty picks the nodes with largest uncertainty, which is equivalent to sampling the boundary of cluster 2. (b) DiverseUncertainty diversifies the clustered nodes, and samples the boundary of both clusters.

209 Before presenting the theory we illustrate the operation of our method and **MaxUncertainty** in Fig-
 210 ure 2. *ScatterSample* first clusters the samples on the propagated feature space (blue circles in
 211 Figure 2), and selects the nodes closest to the cluster centers for initial training (green stars in
 212 Figure 2). Then, during the dynamic sampling steps, we compute the uncertainty using equation 4.
 213 MaxUncertainty approach will select the nodes with the largest uncertainty. Under our setup, it is
 214 equivalent to sample nodes at the boundary of the largest cluster since the distance to the cluster
 215 center is the most important factor of uncertainty (Figure 2(a)). While DiverseUncertainty will
 216 diversify the high uncertainty nodes, which is equivalent to sample from the boundary of each cluster
 217 (Figure 2(b)). The red stars of Figure 2 show the nodes labeled during the uncertainty sampling stage.
 218 Since MaxUncertainty algorithm only labels the nodes in cluster 2, cluster 1 is ignored the prediction
 219 uncertainty of cluster 2 cannot be reduced. On the contrary, DiverseUncertainty samples nodes from
 220 both cluster 1 and 2. Thus, it could reduce the prediction uncertainty in both clusters.

221 Then, the following theorem quantifies the relationship of the MSEs of both algorithms under the
 222 setup of Sec. 5.1.

223 **Theorem 5.1.** Consider a case where feature dimension $d = 1$. With the above notation
 224 and assumptions, let $r_i = \exp\left[-\frac{d_i^2}{2\theta}\right]$. If we satisfy $d_m^2 \geq d_{m-1}^2 + 4\log\theta$ and $\delta \geq d_m +$
 225 $\max\left(\sqrt{d_m^2 + \theta \log(9m)}, 2\theta \log\left(\frac{3\sqrt{m}}{1-r_m}\right)\right)$, we have

$$\frac{MSE(f(x)|MaxUncertainty)}{MSE(f(x)|DiverseUncertainty)} \geq \frac{1}{2(1+\tau)} \frac{1+r_m^2}{1-r_m} - \frac{8}{3} = \frac{1}{\tau+1} O(\theta).$$

226 *Proof:* The complete proof is included in Appendix B.

227 Theorem 5.1 suggests that when the GP function is smooth enough (large θ), the MaxUncertainty
 228 will have larger MSE than the MaxDiversity algorithm (proof is in appendix section B). A large θ
 229 suggests a close correlation between the labels of the nodes that are close to each other. It is also
 230 common for most of the graph datasets where samples clustered together usually have similar labels.
 231 Thus, DiverseUncertainty can achieve a smaller MSE in this case.

Table 1: Statistics of graph datasets used in experiments.

Data	# Nodes	# Train Nods	# Edges	# Classes
Cora	2,708	1,208	5,429	7
Citeseer	3,327	1,827	4,732	6
Pubmed	19,717	18,217	44,328	3
Corafull	19,793	18,293	126,842	70
ogbn-products	2,449,029	196,615	61,859,149	47

232 6 Experiments

233 We evaluate the performance of *ScatterSample* on five different datasets.

Datasets. We evaluated the different methods on the Cora, Citeseer, Pubmed, Corafull [KW16], and ogbn-products [Hu+20] datasets (Table 1). Besides the ogbn-products, we do not keep original data split of the training and testing set. For the nodes that are not in the validation or testing sets (the validation and testing sets follows the split in the dgl package “dgl.data” [Wan+19]), we will add them to the training set. The labels can only be queried from the training set.

Baselines. For different sampling budget B , we compare the test accuracy of *ScatterSample* with the following graph active learning baselines:

- *Random sampling.* Select B nodes uniformly at random from \mathcal{V}_{train} .
- *AGE [CZC17]:* AGE computes a score which combines the node centrality, information density, and uncertainty, to select B nodes with the highest scores.
- *ANRMAB [Gao+18]:* ANRMAB learns the combination weights of the three metrics used by AGE with multi-armed bandit method.
- *FeatProp:* FeatProp [Wu+19b] clusters the feature propagations into B clusters and pick the nodes closest to the cluster centers.
- *Grain:* [Zha+21] score the node by the weighted average of the influence score and diversity score. And select the top B nodes with largest node scores. Grain includes two different approaches of selecting nodes, Grain (ball-D) and Grain (NN-D).
- *ScatterSample:* For the sample scale graph dataset (Cora, Citeseer), we set the initial sampling budget to $3\% \cdot |\mathcal{V}_{train}|$ and sample $1\% \cdot |\mathcal{V}_{train}|$ each round during the dynamic sampling period. For medium scale datasets (Pubmed and Corafull), we set the initial sampling budget to $1\% \cdot |\mathcal{V}_{train}|$ and sample $0.5\% \cdot |\mathcal{V}_{train}|$ each dynamic sampling round. For the large scale dataset (ogbn-products), initial sampling budget is $0.2\% \cdot |\mathcal{V}_{train}|$, and each dynamic sampling round selects $0.05\% \cdot |\mathcal{V}_{train}|$ nodes.

GNN setup. We train a 2-layer GCN network with hidden layer dimension = 64 for Cora, Citeseer and Pubmed, and = 128 for Corafull and ogbn-products. To train the GNN, we follow the standard random neighbor sampling where for each node [HYL17], we randomly sample 5 neighbors for the convolution operation in each layer. We use the function in “dgl” package to train the GNNs [Wan+19].

6.1 Performance Results

We compare the performance of different active graph neural network learning algorithms under different labeling budgets (B). We parameterize the labeling budget B equal to a certain proportion of the nodes in the training set ($B = r|\mathcal{V}_{train}|$). For Cora and Citeseer, we vary r from 5% to 15% in increment of 2%; for Pubmed and Corafull, r is varied from 3% to 10%; for ogbn-product dataset, we vary the r from 0.3% to 1%. The performance of the active learning algorithms are measured with the test accuracy.

Accuracy. Figure 3 shows the test accuracy of baselines trained on different proportions of the selected nodes. *ScatterSample* improves the test accuracy and consistently outperforms other baselines in all the datasets. In Citeseer, *ScatterSample* requires 9% of the node labels to achieve test accuracy 74.2%, while the best alternative baselines “Grain (ball-D)” and “Grain (NN-D)” need to label 15% of nodes to achieve similar accuracy, which corresponds to a 40% savings of the labeling cost. Similarly, in PubMed and ogbn-products, *ScatterSample* achieves a 50% labeling cost reduction compared to the best alternative baseline.

Efficiency. Here, we compare the computation time among the methods that use the graph structure and node features to select the samples namely, *ScatterSample*, “Grain (ball-D)” and “Grain (NN-D)”. We use the ogbn-products dataset to perform comparisons. *ScatterSample* takes less than 8 hours to determine the labeling nodes and train the GNN, while the Grain algorithm requires more than 240 hours. Grain requires $\mathcal{O}(n^2)$ complexity to calculate the scores of all nodes, which is prohibitive complexity in large graphs.

Complexity analysis. The computation complexity of DiverseUncertainty is $\mathcal{O}(|E| + r * B_t^2)$. It is because *ScatterSample* includes two parts: 1) computing the node representations with complexity $\mathcal{O}(|E|)$ where $|E|$ is the number of edges and 2) cluster the the uncertain nodes where the complexity is $\mathcal{O}(rB_t^2)$. Since both r and B_t are small, $rB_t^2 < |E|$, our method does not add a lot of extra burden compared to the model training time.

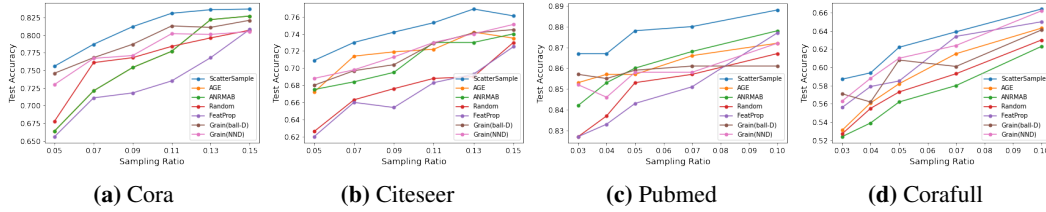


Figure 3: ScatterSample (blue), wins consistently: Comparison of the test accuracy of active GNN learning algorithms at different labeling budget. The x -axis shows # labeled nodes/# nodes in training set.

287 **6.2 Ablation Study**

288 The MaxDiversity algorithm of *ScatterSample* needs to determine the size of candidate set C_t before
 289 selecting a subset S_t from C_t for labeling. Hence, sampling redundancy r and the clustering
 290 algorithm to cluster the nodes in C_t will affect the performance of *ScatterSample*. In this section, we will
 291 evaluate the effect of both factors.

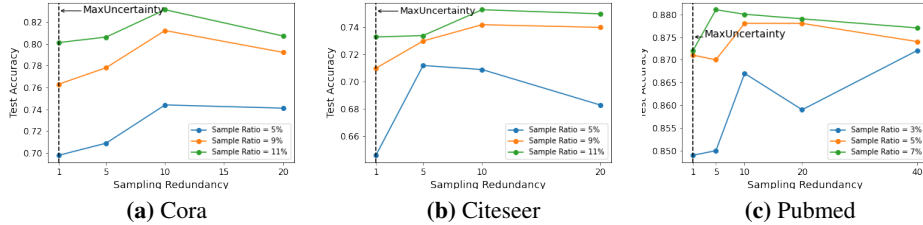


Figure 4: Compare the performance under different sampling redundancy r . When $r = 1$, Diverse-Uncertainty reduces to MaxUncertainty method.

292 **Sampling redundancy r :** Recall from algorithm 1, the sampling redundancy r controls the relative
 293 size of candidate set C_t to size of sampled node S_t . When $r = 1$, *ScatterSample* reduces to the
 294 standard MaxUncertainty algorithm. And figure 4 shows that the sampling the most uncertain nodes
 295 is significantly worse than DiverseUncertainty. For the Citeseer dataset, DiverseUncertainty can
 296 outperform MaxUncertainty by over 7% when sampling ratio is 5%. Therefore, to achieve a good
 297 test accuracy, r should be carefully selected. Figure 4 suggests that as r increases, the test accuracy
 298 quickly boosts at the early stage, and then decreases slowly.

299 **Sensitivity to initial sampling ratio:** During the initial sampling stage, DiverseUncertainty samples
 300 B_0 nodes to train the model initially. And the initially trained model will affect the nodes sampled
 301 during the dynamic sampling period. We test the effect of different initial sampling ratio on Cora
 302 and Citeseer datasets. We vary the initial sampling ratio from 2% to 4%, and figure A5 shows that
 303 DiverseUncertainty is robust to the choice of initial sampling ratio.

304 **Diverse uncertainty algorithms:** Besides the sampling algorithm used by DiverseUncertainty,
 305 there are some other algorithms to pick the representative nodes from the candidate set S_t . First, we
 306 will evaluate three algorithms to cluster and select the propagated features.

- 307 • Random select: randomly pick nodes S_t from C_t .
- 308 • DiverseUncertainty: use k -means++ to cluster the nodes in C_t and
- 309 • Random round-robin Algorithm [Cit+21]: use the cluster labels from the initial sampling period
 310 (the initial sampling period clusters all the nodes in V_{train}). Then, following the Algorithm A3
 311 (see Appendix) to select S_t from C_t

312 Figure A6 suggests that k -means++ clustering algorithm achieves a better test accuracy in most
 313 cases compared to random selection or random round-robin algorithm (see Appendix). Moreover,
 314 compared to random sampling algorithm, k -means++ clustering algorithm is more robust when the
 315 sampling ratio increases. As the sampling ratio increases, the test accuracy of k -means++ keeps
 316 increasing in most cases, while the test accuracy of random sampling algorithm has more fluctuations.

Another factor that affects the test performance is the metric for clustering. Besides the propagated features (which is used by MaxDiversity), we can also cluster the input features or the embedding vectors. Since the GNN models typically used do not have a fully connected layer connecting to the output, we cannot use the output of second last layer as the embedding. Hence, we use the GNN output as the embedding vector for clustering. Figure A7 shows that clustering the propagated features consistently outperforms clustering the other two targets. Especially for the ‘‘Citeseer’’ dataset, clustering the propagated features outperforms by at most 5%. To conclude, the k -means++ clustering algorithm achieves the best performance compared to the other selection methods and clustering the propagated features is better than clustering other targets. Thus, DiverseUncertainty uses k -means++ to cluster the propagated features to pick S_t from C_t .

7 Empirical validation of theorem

In this section, we perform simulation analysis to demonstrate that *ScatterSample* can reduce the MSE compared to greedy uncertainty sampling approach.

Graph Simulation Setup. Let the dimension of input feature $d = 1$. Simulate \mathbf{X} from two different clusters, where $(X|C_1) \sim Uniform(-15, -5)$ and $(X|C_2) \sim Uniform(8, 12)$. In our simulation, we randomly generated 100 nodes for each cluster. Each node is randomly connected to two other nodes in the same cluster. Moreover, for the edges between clusters, we set a probability threshold r such that $P[V_i \in C_1 \text{ connect to a node } \in C_2] = r$ (See Appendix D for details).

Label of nodes. The label of a node depends on its propagated features. First compute the 1-layer feature propagation of each node, $\mathbf{X}^{(1)}$. Then, the label of i -th node is $y_i = |X_i^{(1)}|^2$. Here, because the two cluster centers are equally distanced from 0, hence, the label function is also symmetric around 0.

Node sampling. During the initial sampling step, label the nodes closest to the cluster centers and train the GP function. To sample uncertain nodes,

- MaxUncertainty: Label the 8 nodes with largest uncertainty.
- DiverseUncertainty: Collect the top 80 nodes with largest uncertainty into the candidate set. Then, use k -means++ to cluster the nodes in the candidate set into 8 clusters. Label the 8 nodes closest to the cluster centers.

MaxUncertainty and DiverseUncertainty use the newly labeled nodes to update the GP function respectively. Finally, the trained GP function predicts the node labels, and we compute the corresponding MSE.

Figure A8 in the Appendix suggests that MaxUncertainty has larger MSE compared to DiverseUncertainty algorithm. For the MaxUncertainty algorithm, since most of the labeled nodes come from the cluster 1, the MSE of cluster 1 is significantly smaller than that of cluster 2. While for the DiverseUncertainty algorithm, the MSE of cluster 1 and 2 are comparable. As r increases, there are more and more edges between clusters, and the propagated features are less separated. Hence, there are some high uncertainty nodes from cluster 1 very close to cluster 2, which is beneficial for MaxUncertainty to learn the labels of nodes from cluster 2. Thus, we could observe $\frac{\text{MSE of MaxUncertainty}}{\text{MSE of DiverseUncertainty}}$ keeps decreasing when r increases. When r is very large, cluster 1 and 2 will merge into one cluster, and MSEs of both methods no longer have a significant difference.

8 Conclusion

Learning a GNN model with limited labeling budget is an important but challenging problem. In this paper:

- We propose a novel data efficient GNN learning algorithm, *ScatterSample*, which efficiently diversifies the uncertain nodes and achieves better test accuracy than recent baselines.
- We provide theoretical guarantees: Theorem 5.1 proves the advantage of *ScatterSample* over MaxUncertainty sampling.
- Experiments on real data show that *ScatterSample* can save up to 50% labeling size, for the same test accuracy.

We envision *ScatterSample* will inspire future research of combining uncertainty sampling and representation sampling (diversifying).

References

- 368 [AV06] D. Arthur and S. Vassilvitskii. *k-means++: The advantages of careful seeding*. Tech. rep. Stanford, 2006
- 369 [Bro+17] M. M. Bronstein, J. Bruna, Y. LeCun, A. Szlam, and P. Vandergheynst. “Geometric
370 deep learning: going beyond euclidean data”. In: 34.4 (2017), pp. 18–42
- 371 [CZC17] H. Cai, V. W. Zheng, and K. C.-C. Chang. “Active learning for graph embedding”. In:
372 *arXiv preprint arXiv:1705.05085* (2017)
- 373 [Cit+21] G. Citovsky, G. DeSalvo, C. Gentile, L. Karydas, A. Rajagopalan, A. Rostamizadeh,
374 and S. Kumar. “Batch Active Learning at Scale”. In: *Advances in Neural Information
375 Processing Systems* 34 (2021)
- 376 [DBV16] M. Defferrard, X. Bresson, and P. Vandergheynst. “Convolutional neural networks on
377 graphs with fast localized spectral filtering”. In: Barcelona, Spain, 2016, pp. 3844–3852
- 378 [DP18] M. Ducoffe and F. Precioso. “Adversarial active learning for deep networks: a margin
379 based approach”. In: *arXiv preprint arXiv:1802.09841* (2018)
- 380 [Gao+18] L. Gao, H. Yang, C. Zhou, J. Wu, S. Pan, and Y. Hu. “Active discriminative network rep-
381 resentation learning”. In: *IJCAI International Joint Conference on Artificial Intelligence*.
382 2018
- 383 [HYL17] W. L. Hamilton, R. Ying, and J. Leskovec. “Inductive representation learning on large
384 graphs”. In: *Proceedings of the 31st International Conference on Neural Information
385 Processing Systems*. 2017, pp. 1025–1035
- 386 [Han+14] S. Hanneke et al. “Theory of disagreement-based active learning”. In: *Foundations and
387 Trends® in Machine Learning* 7.2-3 (2014), pp. 131–309
- 388 [Hu+20] W. Hu, M. Fey, M. Zitnik, Y. Dong, H. Ren, B. Liu, M. Catasta, and J. Leskovec.
389 “Open Graph Benchmark: Datasets for Machine Learning on Graphs”. In: *arXiv preprint
390 arXiv:2005.00687* (2020)
- 391 [IMG20] V. N. Ioannidis, A. G. Marques, and G. B. Giannakis. “Tensor Graph Convolutional
392 Networks for Multi-Relational and Robust Learning”. In: *IEEE Transactions on Signal
393 Processing* 68 (2020), pp. 6535–6546
- 394 [KW16] T. N. Kipf and M. Welling. “Semi-supervised classification with graph convolutional
395 networks”. In: *arXiv preprint arXiv:1609.02907* (2016)
- 396 [KVAG19] A. Kirsch, J. Van Amersfoort, and Y. Gal. “Batchbald: Efficient and diverse batch
397 acquisition for deep bayesian active learning”. In: *Advances in neural information
398 processing systems* 32 (2019), pp. 7026–7037
- 399 [O’H78] A. O’Hagan. “Curve fitting and optimal design for prediction”. In: *Journal of the Royal
400 Statistical Society: Series B (Methodological)* 40.1 (1978), pp. 1–24
- 401 [See04] M. Seeger. “Gaussian processes for machine learning”. In: *International journal of
402 neural systems* 14.02 (2004), pp. 69–106
- 403 [Set09] B. Settles. “Active learning literature survey”. In: (2009)
- 404 [THTS05] G. Tur, D. Hakkani-Tür, and R. E. Schapire. “Combining active and semi-supervised
405 learning for spoken language understanding”. In: *Speech Communication* 45.2 (2005),
406 pp. 171–186
- 407 [Vel+17] P. Veličković, G. Cucurull, A. Casanova, A. Romero, P. Lio, and Y. Bengio. “Graph
408 attention networks”. In: *arXiv preprint arXiv:1710.10903* (2017)
- 409 [Wan+19] M. Wang et al. “Deep Graph Library: A Graph-Centric, Highly-Performant Package for
410 Graph Neural Networks”. In: *arXiv preprint arXiv:1909.01315* (2019)
- 411 [Wu+19a] F. Wu, A. Souza, T. Zhang, C. Fifty, T. Yu, and K. Weinberger. “Simplifying graph
412 convolutional networks”. In: *International conference on machine learning*. PMLR.
413 2019, pp. 6861–6871
- 414 [Wu+19b] Y. Wu, Y. Xu, A. Singh, Y. Yang, and A. Dubrawski. “Active learning for graph neural
415 networks via node feature propagation”. In: *arXiv preprint arXiv:1910.07567* (2019)
- 416 [Zha+21] W. Zhang, Z. Yang, Y. Wang, Y. Shen, Y. Li, L. Wang, and B. Cui. “Grain: Improving
417 data efficiency of graph neural networks via diversified influence maximization”. In:
418 *arXiv preprint arXiv:2108.00219* (2021)
- 419 [ZG02] X. Zhu and Z. Ghahramani. “Learning from labeled and unlabeled data with label
420 propagation”. In: (2002)
- 421
- 422

423 A Estimation and prediction of the GP model

424 Given the assumptions and notations above, the likelihood of GP model can be written as:

$$f(\mathbf{y} \mid \mu, \sigma^2, \boldsymbol{\theta}) \propto \exp \left[-\frac{1}{2\sigma^2} (\mathbf{y} - \mathbf{1}\mu)^T \mathbf{K}(\mathbf{X}^{(k)})^{-1} (\mathbf{y} - \mathbf{1}\mu) \right].$$

425 Here, we assume $\boldsymbol{\theta} = (\theta_1, \theta_2, \dots, \theta_d)$ is a known parameter, and only μ and σ^2 are left to fit. The
 426 MLE of μ and σ^2 are, $\hat{\mu} = \sum_{i=1}^n \mathbf{y}_i$ and $\hat{\sigma}^2 = \frac{1}{n} (\mathbf{y} - \hat{\mu})^T \mathbf{K}(\mathbf{X}^{(k)})^{-1} (\mathbf{y} - \hat{\mu})$.

427 Given a testing point $\mathbf{x}_*^{(k)}$, by the GP model fitted by D , the prediction of the response $f(\mathbf{x}_*^{(k)}) \sim$
 428 $N(\mu^*, \sigma^{*2})$, where

$$\begin{aligned} \mu^* &= \mu + \mathbf{k}^{*T} \mathbf{K}(\mathbf{X}^{(k)})^{-1} (\mathbf{y} - \mathbf{1}\hat{\mu}) \quad \text{and} \quad \sigma^{*2} = \hat{\sigma}^2 (1 - \mathbf{k}^{*T} \mathbf{K}(\mathbf{X}^{(k)}) \mathbf{k}^*) \\ \mathbf{k}^* &= [K(\mathbf{x}_1, \mathbf{x}^*), K(\mathbf{x}_2, \mathbf{x}^*), \dots, K(\mathbf{x}_n, \mathbf{x}^*)]^T \in \mathbb{R}^{n \times 1} \end{aligned} \quad (4)$$

429 B Proof of theorem 1

430 Before proving theorem 5.1, we first provide some preliminary results of Gaussian kernel matrix.

431 B.1 Preliminary of Gaussian kernel matrix

432 **Lemma B.1.** *Let \mathbf{K} be the Gaussian kernel matrix of vector $(\mathbf{c}_1, \mathbf{c}_2, \dots, \mathbf{c}_m)$. Since*
 433 *$\min_{i \neq j} \|\mathbf{c}_i - \mathbf{c}_j\| > \delta$, we have $\mathbf{K}_{ij} < \exp \left[-\frac{\delta^2}{\theta} \right]$. Denote $\epsilon = \exp \left[-\frac{\delta^2}{\theta} \right]$. Then, $K_{ij}^{-1} > -\epsilon$ if*
 434 *$i \neq j$, and $1 < K_{ii}^{-1} < 1 + (m-1)\epsilon^2$.*

435 *Proof.* Let $\mathbf{K} = \mathbf{I} + \mathbf{A}$. By Neumann series, $\mathbf{K}^{-1} = \mathbf{I} + \sum_{t=1}^{\infty} (-1)^t \mathbf{A}^t$. Thus, $\mathbf{K}_{ij} > -\mathbf{A}_{ij} > -\epsilon$
 436 for $i \neq j$, and $1 < \mathbf{K}_{ii} < 1 + \mathbf{A}_{ii}^2 < 1 + (m-1)\epsilon^2$ \square

437 B.2 Prove MaxUncertainty method samples $2m$ from cluster m

438 During the initial sampling stage, the nodes at the cluster centers are sampled. Then, the variance of a
 439 sample x is,

$$\text{Var}(f(x)) = \sigma^2 (1 - \mathbf{k}^T \mathbf{K}^{-1} \mathbf{k}), \quad (5)$$

440 where $\mathbf{k} = (K(x, c_1), K(x, c_2), \dots, K(x, c_m))$ and $\mathbf{K} = \mathbf{K}(\mathbf{c})$ is the Gaussian kernel matrix of
 441 $\mathbf{c} = (c_1, c_2, \dots, c_m)$.

442 For a node x from cluster i , the $\text{Var}(f(x))$ is monotone increasing as x moves from cluster center
 443 to boundary. Let $\omega = \exp \left[-\frac{(\delta - d_m)^2}{2\theta} \right]$. Since $|x - c_j| \geq \delta - d_i \geq \delta - d_m$ for $j \neq i$, naturally, we
 444 have $\omega < \mathbf{k}_j$. Then, following lemma B.1,

$$\mathbf{k}(x, \mathbf{c})^T \mathbf{K}^{-1} \mathbf{k}(x, \mathbf{c}) \geq \exp \left[-\frac{d_i^2}{\theta} \right] \mathbf{K}_{ii}^{-1} > \exp \left[-\frac{d_i^2}{\theta} \right] \quad (6)$$

445 With equation 6, we can upper bound the variance of the x from cluster i .

446 In the next step, we **lower bound the variance of x at the boundary of cluster m** (largest cluster),
 447 and show that its variance is strictly larger than nodes from other clusters.

$$\mathbf{k}(x, \mathbf{c})^T \mathbf{K}^{-1} \mathbf{k}(x, \mathbf{c}) < \left(\exp \left[-\frac{d_m^2}{\theta} \right] + (m-1)\omega^2 \right) [1 + (m-1)\epsilon^2], \quad (7)$$

448 Since $\delta \geq d_m + \sqrt{d_m^2 + \theta \log(9m)}$, we have $(m-1)\epsilon^2 < (m-1)\omega^2 \leq \frac{1}{9} \exp \left[-\frac{d_m^2}{\theta} \right] <$
 449 $\frac{1}{9} \exp \left[-\frac{d_i^2}{\theta} \right]$.

$$\begin{aligned}
 \text{RHS of equation 7} &\leq 2 \left(\exp \left[-\frac{d_m^2}{\theta} \right] + (m-1)\omega^2 \right) \\
 &\leq \frac{1}{2} \exp \left[-\frac{d_i^2}{\theta} \right] + 2(m-1)\omega^2 < \frac{13}{18} \exp \left[-\frac{d_i^2}{\theta} \right] \quad (8)
 \end{aligned}$$

450 The RHS of equation 7 is strictly smaller than the LHS of equation 6. Therefore, the uncertainty of
 451 nodes at the boundary of cluster m is larger than the uncertainty of nodes from other clusters. For
 452 our case, feature dimension is 1 and there only exist 2 points at the boundary of cluster m . However,
 453 since the nodes are continuous distributed, MaxUncertainty will pick the other $2(m-1)$ nodes close
 454 to the boundary of cluster m .

455 B.3 Bound the MSE of MaxUncertainty and DiverseUncertainty

456 From previous section, we have seen the boundary nodes of cluster m have the largest uncertainty.
 457 Thus, MaxUncertainty will sample $2m$ nodes from the cluster m . To lower bound the MSE of
 458 MaxUncertainty, we consider the other $(m-1)$ clusters. Since the Gaussian Process model does not
 459 have noise, MSE of the prediction is equal to its variance.

460 Let $\mathbf{h} = (\mathbf{c}, \mathbf{s}) \in \mathbb{R}^{3m}$, where \mathbf{h} are the sampled nodes and $\mathbf{s} \in \mathbb{R}^{2m}$ are the $2m$ nodes sampled
 461 during the dynamic sampling stage. Denote $\mathbf{K}(\mathbf{h})$ to be Gaussian kernel matrix of \mathbf{h} . Let $t = |x - c_i|$
 462 be the distance from node x to its cluster center.

$$\begin{aligned}
 \mathbf{k}(x, \mathbf{h})^T \mathbf{K}^{-1}(\mathbf{h}) \mathbf{k}(x, \mathbf{h}) &\leq [1 + m\epsilon^2 + 2m\omega^2] \left(\exp \left[-\frac{t^2}{\theta} \right] + 3m\omega^2 \right) \\
 &\leq (1 + 3m\omega^2) \left(\exp \left[-\frac{t^2}{\theta} \right] + 3m\omega^2 \right) \quad (9)
 \end{aligned}$$

463 Moreover, we have $\mathbb{E}_t \left(\exp \left[-\frac{t^2}{\theta} \right] \right) \leq \frac{1}{2} \left(1 + \exp \left[-\frac{d_m^2}{\theta} \right] \right)$. Let $r_i = \exp \left[-\frac{d_i^2}{4\theta} \right]$ and $a =$
 464 $\exp \left[-\frac{d_m^2}{\theta^*} \right]$, we have

$$\text{MSE}(f(x) \mid \text{MaxUncertainty}, x \in \mathcal{S}_i) > \sigma^2 \left[\left(\frac{1}{2} - \frac{a}{2} - \frac{a^2}{9} \right) - \left(\frac{1}{2} + \frac{a}{6} \right) r_i^4 \right]. \quad (10)$$

465 Hence, $\text{MSE}(f(x) \mid \text{MaxUncertainty}) > \sigma^2 \sum_{i=1}^{m-1} \frac{d_i^2}{\|\mathbf{d}\|^2} \left[\left(\frac{1}{2} - \frac{a}{2} - \frac{a^2}{9} \right) - \left(\frac{1}{2} + \frac{a}{6} \right) r_i^4 \right]$. Let
 466 $h(r_i^2) = \left(\frac{1}{2} - \frac{a}{2} - \frac{a^2}{9} \right) - \left(\frac{1}{2} + \frac{a}{6} \right) r_i^4$ and h is concave in d_i^2 . Thus,

$$h(r_m^2) = \left(\frac{1}{2} - \frac{a}{2} - \frac{a^2}{9} \right) - \left(\frac{1}{2} + \frac{a}{6} \right) r_i^4 \leq \tau \sum_{i=1}^{m-1} \frac{h(r_i^2)}{r_m^2} h(r_m^2) \leq \tau \sum_{i=1}^{m-1} h(r_i^2). \quad (11)$$

467 Hence, $\text{MSE}(f(x) \mid \text{MaxUncertainty}) > \frac{\sigma^2}{1+\tau} \sum_{i=1}^m \frac{d_i^2}{\|\mathbf{d}\|^2} \left[\left(\frac{1}{2} - \frac{a}{2} - \frac{a^2}{9} \right) - \left(\frac{1}{2} + \frac{a}{6} \right) r_i^4 \right]$.

468 Then, we upper bound the MSE of DiverseUncertainty. Since each cluster labels 2 nodes at the
 469 cluster boundary. For node x from cluster i , the distance between node i to the closest labeled point
 470 is smaller than $\frac{d_i}{2}$. Hence,

$$\mathbf{k}(x, \mathbf{h})^T \mathbf{K}^{-1}(\mathbf{h}) \mathbf{k}(x, \mathbf{h}) \geq \exp \left[-\frac{t^2}{\theta} \right] + \exp \left[-\frac{(d_i - t)^2}{\theta} \right] - 2 \exp \left[-\frac{d_i^2}{\theta} \right] \exp \left[-\frac{t^2 + (d_i - t)^2}{2\theta} \right] \geq \frac{2r_i}{1 + r_i^2}. \quad (12)$$

471 Thus, we have $MSE(f(x) | DiverseUncertainty, x \in \mathcal{S}_i) \leq \sigma^2 \frac{(1-r_i)^2}{1+r_i^2}$ and $MSE(f(x) |$
 472 $DiverseUncertainty) \leq \sigma^2 \sum_{i=1}^m \frac{d_i^2}{\|\mathbf{d}\|^2} \frac{(1-r_i)^2}{1+r_i^2}$.

473 Moreover, $\frac{MSE(f(x)|MaxUncertainty, x \in \mathcal{S}_i)}{MSE(f(x)|DiverseUncertainty, x \in \mathcal{S}_i)} \geq \frac{1+r_i^2}{1-r_i} (\frac{1}{2} + \frac{a}{6}) - \frac{(1+r_i^2)}{(1-r_i)^2} (\frac{2a}{3} + \frac{a^2}{9})$. Since
 474 $\delta \geq d_m + 2\theta \log(\frac{3\sqrt{m}}{1-r_m})$, we have $a \leq (1-r_i)^2$ for all $i = 1, 2, \dots, m$. Thus,
 475 $\frac{MSE(f(x)|MaxUncertainty, x \in \mathcal{S}_i)}{MSE(f(x)|DiverseUncertainty, x \in \mathcal{S}_i)} \geq \frac{1}{2} \frac{1+r_i^2}{1-r_i} - \frac{8}{3} \geq \frac{1}{2} \frac{1+r_m^2}{1-r_m} - \frac{8}{3}$.

476 Now, we could lower bound $\frac{MSE(f(x)|MaxUncertainty)}{MSE(f(x)|DiverseUncertainty)}$ over the whole sample space, where

$$\frac{MSE(f(x) | MaxUncertainty)}{MSE(f(x) | DiverseUncertainty)} \geq \frac{1}{2(1+\tau)} \frac{1+r_m^2}{1-r_m} - \frac{8}{3}$$

477 Moreover, when θ is large, $r_i = \exp\left[-\frac{d_i^2}{4\theta}\right] \approx 1 - \frac{d_i^2}{4\theta}$. Thus, $\frac{MSE(f(x)|MaxUncertainty)}{MSE(f(x)|DiverseUncertainty)} \geq$
 478 $\frac{1}{1+\tau} O(\theta)$.

479 C Ablation Experiments

480 C.1 Detail of round-robin algorithm

Algorithm 3 Random Round-robin Algorithm

- 1: Input: cluster labels of node i (node $i \in \mathcal{V}_{train}$) cl_n , where $cl_n \in 1, 2, \dots, m$; candidate set \mathcal{C}_t ; number of nodes to label B_t .
 - 2: Using the cluster labels to split \mathcal{C}_t onto clusters A_1, A_2, \dots, A_m . Without loss of generality, $|A_1| \leq |A_2| \leq \dots \leq |A_m|$.
 - 3: $S_t = \emptyset$
 - 4: **for** $i = 1, 2, \dots, B_t$ **do**
 - 5: **for** $j = 1, 2, \dots, m$ **do**
 - 6: **if** $A_j \neq \emptyset$ **then**
 - 7: Uniformly select x from A_j at random
 - 8: $A_j \leftarrow A_j \setminus \{x\}, S_t \leftarrow S_t \cup \{x\}$
 - 9: **break**
 - 10: **end if**
 - 11: **end for**
 - 12: **end for**
 - 13: return S_t
-

481 C.2 Sensitivity to initial sampling ratio

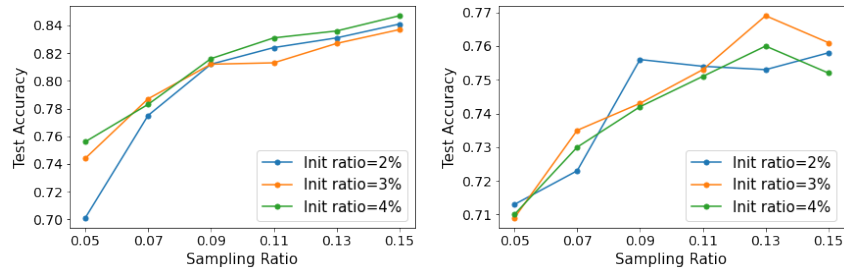


Figure 5: Compare different initial sampling ratios for Cora (left) and Citeseer (Right)

482 **C.3 Compare sampling algorithms**

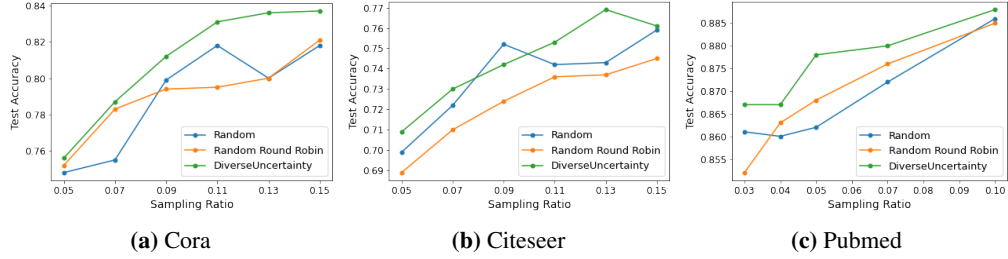


Figure 6: Compare different sampling algorithms to collect S_t from the candidate set C_t .

483 **C.4 Compare clustering algorithms**

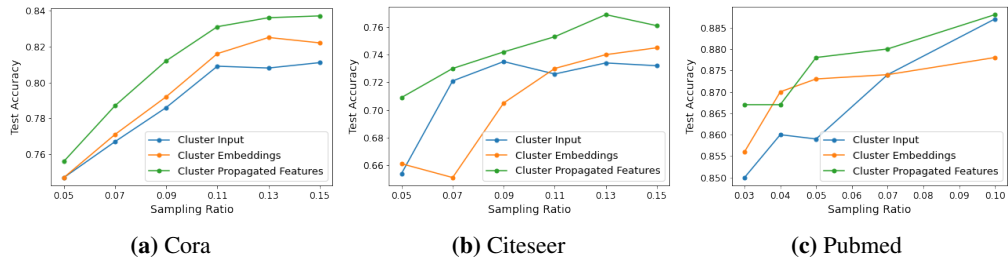


Figure 7: Compare clustering different targets to select S_t from the candidate set C_t .

484 **D Empirical validation of theory**

485 **Graph Simulation Setup.** Let the dimension of input feature $d = 1$. Simulate \mathbf{X} from two different
 486 clusters, where $(X|C_1) \sim Uniform(-15, -5)$ and $(X|C_2) \sim Uniform(8, 12)$. In our simulation,
 487 we randomly generated 100 nodes for each cluster. Then, we simulate the edges between nodes.
 488 The edges can be divided into two categories, edges within clusters and edges between clusters. To
 489 simulate the edges within clusters, for each node, we random select two other nodes from the same
 490 cluster as its neighbor. For the edges between clusters, we set a probability threshold r such that
 491 $P[V_i \in C_1 \text{ connect to a node } \in C_2] = r$. For each node $V_i \in C_1$, generate an indicator variable
 492 $I_i \sim Bernoulli(r)$ to determine whether V_i is connected to cluster 2 (V_i is connected to cluster 2 if
 493 $I_i = 1$). If V_i is connected to cluster 2, randomly pick a node from cluster 2 and connect it to V_i .

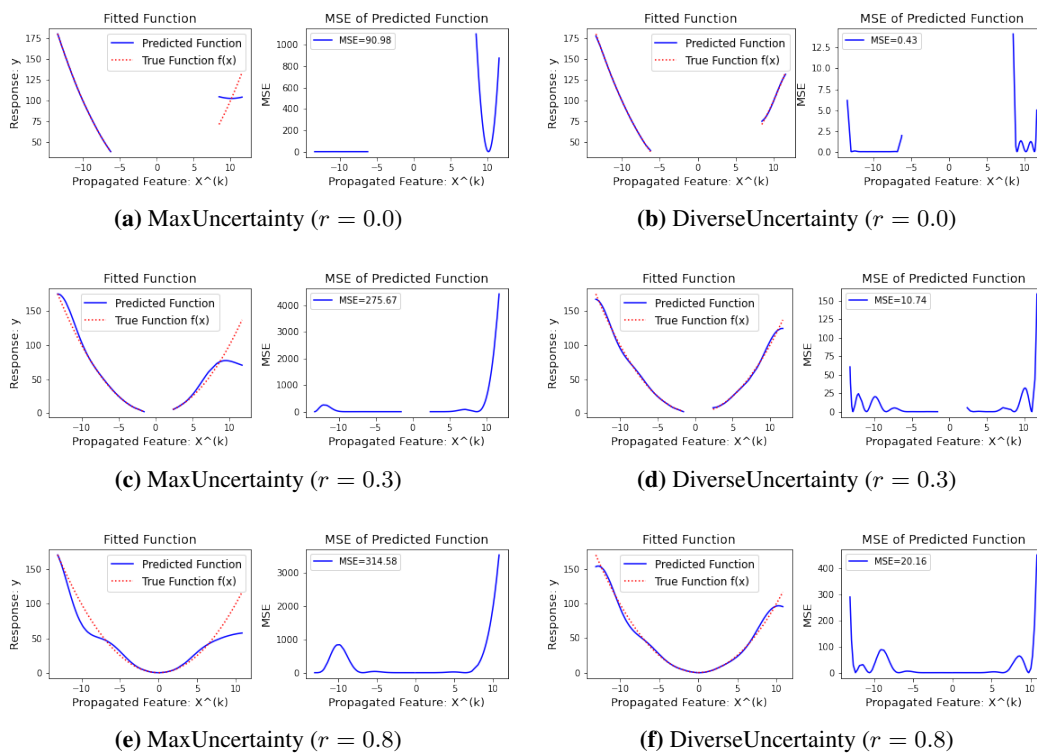


Figure 8: Compare the MSEs of Uncertainty and DiverseUncertainty algorithms under different correlation levels between clusters.